Improved cardiac T-1 mapping accuracy and precision with a new hybrid MOLLI and SASHA technique: MOSHA

Sohani, M.; Geest, R.J.J. van der; Maier, A.; Powell, A.J.J.; Moghari, M.H.H.

Magnetic Resonance Imaging 89 (2022) 33–41

Contents lists available at ScienceDirect

Magnetic Resonance Imaging

journal homepage: www.elsevier.com/locate/mri

Improved cardiac T_1 mapping accuracy and precision with a new hybrid MOLLI and SASHA technique: MOSHA

Majid Sohani [a,c,*], Rob J. van der Geest [b], Andreas Maier [c], Andrew J. Powell [a], Mehdi H. Moghari [a]

[a] Department of Cardiology, Boston Children's Hospital, Department of Pediatrics, Harvard Medical School, USA
[b] Division of Image Processing, Department of Radiology, Leiden University Medical Center, the Netherlands
[c] Department of Pattern Recognition, University of Erlangen-Nuremberg, Germany

ARTICLE INFO

Keywords:
Cardiac magnetic resonance
Tissue characterization
Myocardial fibrosis
Extracellular volume fraction
T_1 mapping

ABSTRACT

Purpose: To develop and validate a new myocardial T_1 mapping sequence (MOSHA) which is based on a combination of the modified Look-Locker inversion recovery (MOLLI) and the saturation recovery single-shot acquisition (SASHA) sequences.

Methods: Prior studies have shown that myocardial T_1 mapping by SASHA is more accurate but less precise than MOLLI. A new myocardial T_1 mapping technique (MOSHA) based on single-shot acquisitions is developed by combining the MOLLI and SASHA sequences. Phantom and patient studies on 15 patients (9 males, median age 21 years) were performed to validate and compare MOSHA with the MOLLI and SASHA sequences in terms of accuracy and precision.

Results: In the phantom study, MOSHA was as accurate as SASHA (P-value = 0.88) and as precise as MOLLI (P-value = 0.59). Similar trends were observed in the patient study. Compared to SASHA, MOSHA accuracy was comparable for blood pre-contrast (P-value$\geq$0.10) and post-contrast (P-value$\geq$0.70), and for myocardium pre-contrast (P-value = 0.70) and post-contrast (P-value = 0.09). Compared to MOLLI, MOSHA precision was lower for blood pre-contrast (P-value$<$0.01) and higher for blood post-contrast (P-value$\leq$0.01), and comparable for myocardium pre-contrast (P-value = 0.24) and post-contrast (P-value = 0.07). Synthetic Extracellular volume fraction (ECV) calculated by MOSHA was more precise than those of SASHA and MOLLI (P-value$\leq$0.01).

Conclusion: In phantom studies and patients, MOSHA has comparable accuracy as SASHA and nearly similar precision as MOLLI for T_1 mapping. Precision of MOSHA was better than MOLLI and SASHA in synthetic ECV measurements. Therefore, it may be a superior choice in clinical practice for a precise and accurate calculation of T_1 and ECV.

1. Introduction

The measurement of longitudinal magnetization relaxation time (T_1) is a known cardiovascular magnetic resonance (CMR) technique that is used for quantitative tissue characterization [1–4]. T_1 mapping pre- and post-contrast can be useful in detecting diffuse myocardial fibrosis by calculating the extracellular volume fraction (ECV) [5]. Myocardial T_1 and ECV can be helpful in diagnosing a variety of heart diseases including myocarditis, stress-induced cardiomyopathy, acute and chronic myocardial infarction, cardiac amyloidosis, rheumatoid arthritis, systemic sclerosis, Anderson-Fabry disease, and diffuse fibrosis [2–4].

Different T_1 mapping sequences based on inversion recovery (i.e., a 180° pulse) [6–10], saturation recovery (i.e., a 90° pulse) [11,12], or a combination of these two pulses [13,14] have been developed. The most widely used method is the modified Look-Locker inversion recovery (MOLLI) sequence [7]. It has the advantage of good precision but underestimates T_1 [10,15]. To improve the accuracy of MOLLI, the saturation recovery single-shot acquisition (SASHA) sequence was developed [11]. SASHA has been shown to be more accurate than MOLLI in the estimation of T_1 but has lower precision [10,16].

Accordingly, we sought to develop a new T_1 mapping sequence which is both accurate and precise. Our technique is based on a combination of the MOLLI and SASHA sequences, and thus termed MOSHA.

* Corresponding author at: Department of Cardiology, Boston Children's Hospital, 300 Longwood Avenue, Boston, MA 02115, USA.
E-mail address: majid.sohani@gmail.com (M. Sohani).

https://doi.org/10.1016/j.mri.2022.02.004
Received 27 July 2021; Received in revised form 12 January 2022; Accepted 13 February 2022
Available online 16 February 2022

Phantom and patient studies were performed to compare the accuracy and precision of MOSHA with MOLLI and SASHA.

2. Methods

2.1. Image acquisition

A schematic diagram of the MOLLI, SASHA, and MOSHA sequences is shown in Fig. 1. The typical pre-contrast MOLLI sequence is based on a 5 (3 s)3 scheme [7]. Following an inversion pre-pulse with a delay of ≈110 ms before image acquisition to invert the longitudinal magnetization vector, the T_1 recovery curve is sampled once during each of the next 5 consecutive beats. Next, a 3-s pause interval is applied to allow the longitudinal magnetization vector to recover. After this pause interval, a second inversion pre-pulse with a delay of ≈350 ms to image acquisition is applied in the 9th beat and the T_1 recovery curve is sampled once during each of the next 3 consecutive beats. With SASHA [11], without applying any pre-pulse, an image is acquired in the first beat to sample the T_1 recovery curve at the infinity time point. For each of the next 9 beats, a saturation pre-pulse and T_1 sampling are performed. The pre-pulse delay time is linearly incremented from ≈105 ms to 700 ms with each beat (assumed heart rate of 60 bpm).

Our MOSHA sequence is a combination of MOLLI and SASHA. It is based on a 5(3 s)3 scheme of MOLLI for pre-contrast and a 4(1 s)3(1 s)2 scheme for post-contrast. Twenty-one images are acquired in 21 s assuming a heart rate of 60 bpm to estimate the T_1 recovery curve. In the first beat, there is no pre-pulse and the T_1 recovery curve is sampled at the infinity time point. Then, the conventional 5(3 s)3 scheme (or 4(1 s) 3(1 s)2 scheme) MOLLI sequence is performed in the next 11 beats to sample the T_1 recovery curve following an inversion pre-pulse. Immediately after this and without any pause interval, the SASHA sequence is performed in the next 9 beats to sample the T_1 recovery curve using a saturation pre-pulse.

2.2. T_1 computation

The algorithm to calculate the T_1 recovery curve and T_1 map from the MOSHA images for each patient is shown in Fig. 2. MOSHA images were first registered using an elastic registration algorithm with MASS research software (V2018-EXP, Leiden University Medical Center) to account for possible drifts in respiratory pattern and beat-to-beat variations in cardiac position [17,18]. Next, 3 regions of interest (ROIs) were placed on MOSHA images: 1) left ventricle (LV) blood pool, 2) right ventricle (RV) blood pool, and 3) LV myocardium. The ROI for myocardium was covering the entire septum (i.e., the cardiac muscle around the LV). The ROIs for LV and RV were including the entire blood pool in the LV and RV cavities.

MOSHA images were then divided into two groups: MOLLI part (image numbers 2–9) and SASHA part (image numbers 1 and 10–19). Two T_1 values and maps, one from MOLLI part of MOSHA images and one from SASHA part of MOSHA images, were calculated for each ROI by using a nonlinear least-squares solver with 3 parameters, $\left(A - B\,e^{\frac{-t}{T1}}\right)$, in MATLAB (Release 2016, Mathworks, Natick, MA). Our proposed T_1 calculation method is based on prior studies that show that the T_1 map calculated from SASHA images does not have a bias but it is not precise and that the T_1 map derived from MOLLI images is precise but has a bias [4,10,16,19]. For every subject, the bias is separately calculated for each ROI by subtracting the mean of T_1 value calculated from the SASHA part of MOSHA and the MOLLI part of MOSHA over that ROI. The bias for each subject is then added to the T_1 pixel values derived from MOLLI part of MOSHA to generate a T_1 map which is both accurate and precise.

2.3. Extracellular volume (ECV) calculation

Based on the estimated T_1 maps, an ECV map was calculated using the following formula [20]:

$$ECV = (1 - hematocrit) \times \frac{\left(\frac{1}{T_1}\right)_{myo.post} - \left(\frac{1}{T_1}\right)_{myo.pre}}{\left(\frac{1}{T_1}\right)_{LV\ blood.post} - \left(\frac{1}{T_1}\right)_{LV\ blood.pre}} \quad (1)$$

The hematocrit was simulated using the following formula [21]:

$$Synthetic\ hematocrit_{MOLLI} = \left(866.0 \times \left[{}^{1}/_{T_1}\right]_{LV\ blood.MOLLI\ pre}\right) - 0.1232 \quad (2)$$

2.4. Phantom study

To compare the performance of MOSHA versus MOLLI and SASHA, we used a phantom consisting of 14 tubes containing nickel chloride doped agarose gel with different T_1 and T_2 values. The phantom was imaged using a Philips 1.5 T Achieva-dStream scanner (Philips Medical Systems, Best, the Netherlands) and an anterior and posterior receiver coil array. A spin-echo (SE) sequence was used to calculate the reference T_1 values of each tube. The imaging parameters for the SE sequence were field-of-view 300 × 300 mm, slice thickness 10 mm, spatial resolution 2.0 × 2.0 mm reconstructed to 1.2 × 1.2 mm, echo time (TE) 11 ms, repetition time (TR) 10,000 ms, inversion time 50 ms, and scan time ≈25.2 min with a simulated heart rate of 60 bpm. We repeated the SE sequence with 17 different inversion times ranging from 50 ms to 5000 ms to sample the T_1 recovery curve at different time points. Another SE sequence was also acquired to measure the T_2 recovery curve at 32 time points with the following imaging parameters: field-of-view 300 × 300 mm, slice thickness 10 mm, spatial resolution 2.0 × 2.0 mm reconstructed to 1.2 × 1.2 mm, TE 10 ms (× 32), and TR 10000 ms.

Each of the 3 T_1 mapping techniques (MOLLI, SASHA, and MOSHA) was then acquired for different heart rates of 60, 80, 100, and 120 bpm with the following imaging parameters: steady-state free precession readout, field-of-view 300 × 300 mm, slice thickness 10 mm, spatial resolution 2.0 × 2.0 mm reconstructed to 1.2 × 1.2 mm, TE 0.96 ms, TR 2.1 ms, partial echo 0.85, parallel imaging SENSE ×2, flip angle 35°, bandwidth 1082 Hz, 10 ramp-up pulses, linear profile ordering, phase-encoding lines 75, and temporal resolution 161 ms. The scheme for the MOLLI acquisition was 5(3 s)3 with inversion pulse delays of 110 ms and 350 ms before image acquisition. For the SASHA sequence, the delay between the saturation pulse and imaging was initially 105 ms and was then linearly incremented to the maximum allowable delay. A delay of 10 s was applied between each scan to allow full recovery of the net magnetization vector.

2.5. Patient study

To investigate the performance of MOSHA and compare it with MOLLI and SASHA in clinical practice, we performed a prospective study in patients. Subjects were eligible if they were referred for a contrast-enhanced CMR exam. Our hospital's Committee on Clinical Investigation approved this study, and written informed consent was obtained from all subjects.

From each subject, 2 sets each of MOLLI, SASHA, and MOSHA images were acquired in a mid-ventricular short-axis view during breath-holding before (pre-contrast) and 15 min after the administration of 0.15 mmol/kg gadobutrol contrast (post-contrast). The MOLLI scheme for pre-contrast was 5(3 s)3 and for post-contrast was 4(1 s)3(1 s)2. The SASHA scheme was the same for pre- and post-contrast. The MOLLI part of MOSHA sequence has the same scheme as MOLLI acquisition for the pre- and post-contrast. The scanner, coil, and imaging parameters for MOLLI, SASHA, and MOSHA were the same as in the phantom study.

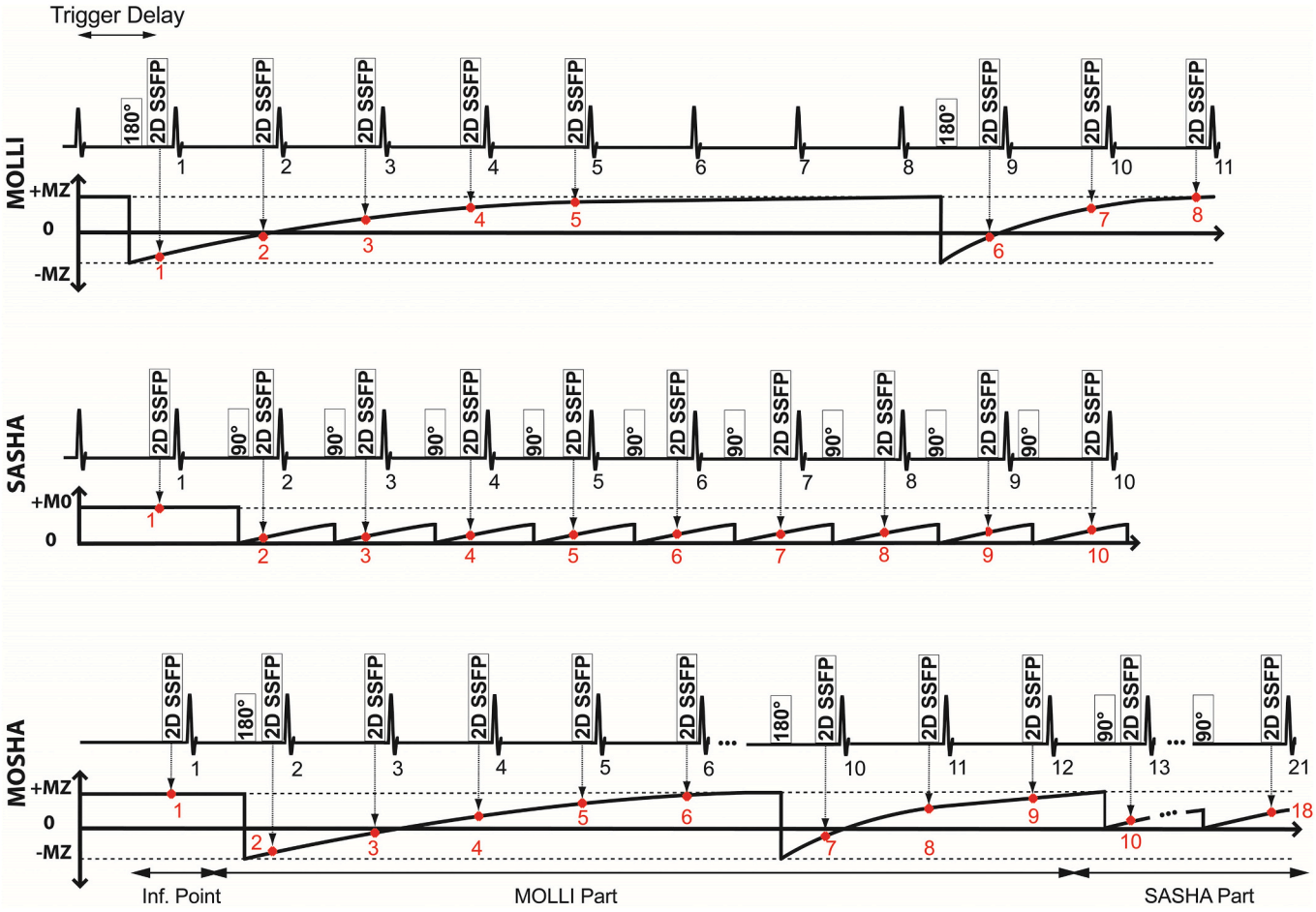

Fig. 1. Schematic diagram of the MOLLI sequence with 5(3 s)3 scheme, the SASHA sequence with 10 beats of image acquisition, and the MOSHA sequence which is the combination of MOLLI and SASHA.

2.6. Statistical analysis

For both the phantom and patient studies, T_1 values for a given ROI were calculated by averaging all the values within the ROI. For the phantom study, the ROI T_1 values calculated from MOLLI, SASHA, and MOSHA were compared with the ones derived from the reference SE images in terms of accuracy and precision. The T_1 values calculated from MOSHA were also compared with MOLLI and SASHA in terms of precision. For the patient study, the pre- and post-contrast ROI T_1 values from MOSHA were compared with SASHA in terms of accuracy and with MOLLI in terms of precision. Bland-Altman plots were also used to compare the pre- and post-contrast T_1 values calculated from MOSHA with SASHA and MOLLI at myocardium and blood pools in the LV and RV cavities. The synthetic ECVs calculated from MOSHA were then compared with the synthetic ECVs from MOLLI and SASHA in terms of accuracy and precision. A paired two-tailed Student's *t*-test was used for all comparisons. A *P*-value ≤ 0.05 was considered to be statistically different.

Accuracy for the phantom study was assessed by calculating the mean difference error defined as the mean of differences between the test method and the reference method $\left(\frac{1}{n}\sum_{i=1}^{n} T_{1\,test,i} - T_{1\,reference,i}\right.$, where $\left.i \text{ is the pixels in the ROI and } n \text{ is the number of tubes}\right)$ [1,16,22]. Precision was defined as the standard deviation in the estimation of T_1 in an ROI $\left(\sqrt{\frac{1}{n-1}\sum_{i=1}^{n}|T_{1i} - \text{mean } T_1|^2}\right.$ where i is the number of pixels in the ROI and n is the total number of pixels in the ROI) [1,16,22].

3. Results

3.1. Phantom study

The measured T_1 using the SE sequence in the 14 tubes of the phantom ranged from 271 to 1484 ms. Fig. 3 shows the T_1 values of the 14 tubes measured from MOLLI, SASHA, and MOSHA images. Fig. 4, Supporting Fig. 1, and Supporting Fig. 2 show the accuracy and precision of MOLLI, SASHA, and MOSHA T_1 measurements at different heart rates using SE T_1 values as the reference. Table 1 lists the mean difference error (a measure of accuracy) and standard deviation (a measure of precision) for T_1 measurement using data from all 4 heart rates and all 14 tubes (i.e., 56 T1 measurements per sequence) and using SE T_1 values as a reference. MOSHA mean difference error for T_1 measurement was similar to SASHA (14.1 ± 42.1 ms vs. 13.2 ± 18.5 ms; *P*-value = 0.88). Specifically, MOLLI T_1 values were systematically lower than those of MOSHA (63.7 ± 55.5 ms vs. 14.1 ± 42.1 ms; *P*-value<0.01). MOSHA T_1 measurement was as precise as MOLLI (8.6 ± 4.9 ms vs. 8.2 ± 3.1 ms; *P*-value = 0.59) and better than SASHA (8.6 ± 4.9 ms vs. 26.6 ± 18.5 ms; *P*-value<0.01).

3.2. Patient study

Fifteen patients (9 males) with a median age of 21 years (range, 2–77) and a median weight of 65 kg (range, 10–80) were enrolled in the study. Their principal diagnoses were bicuspid aortic valve and

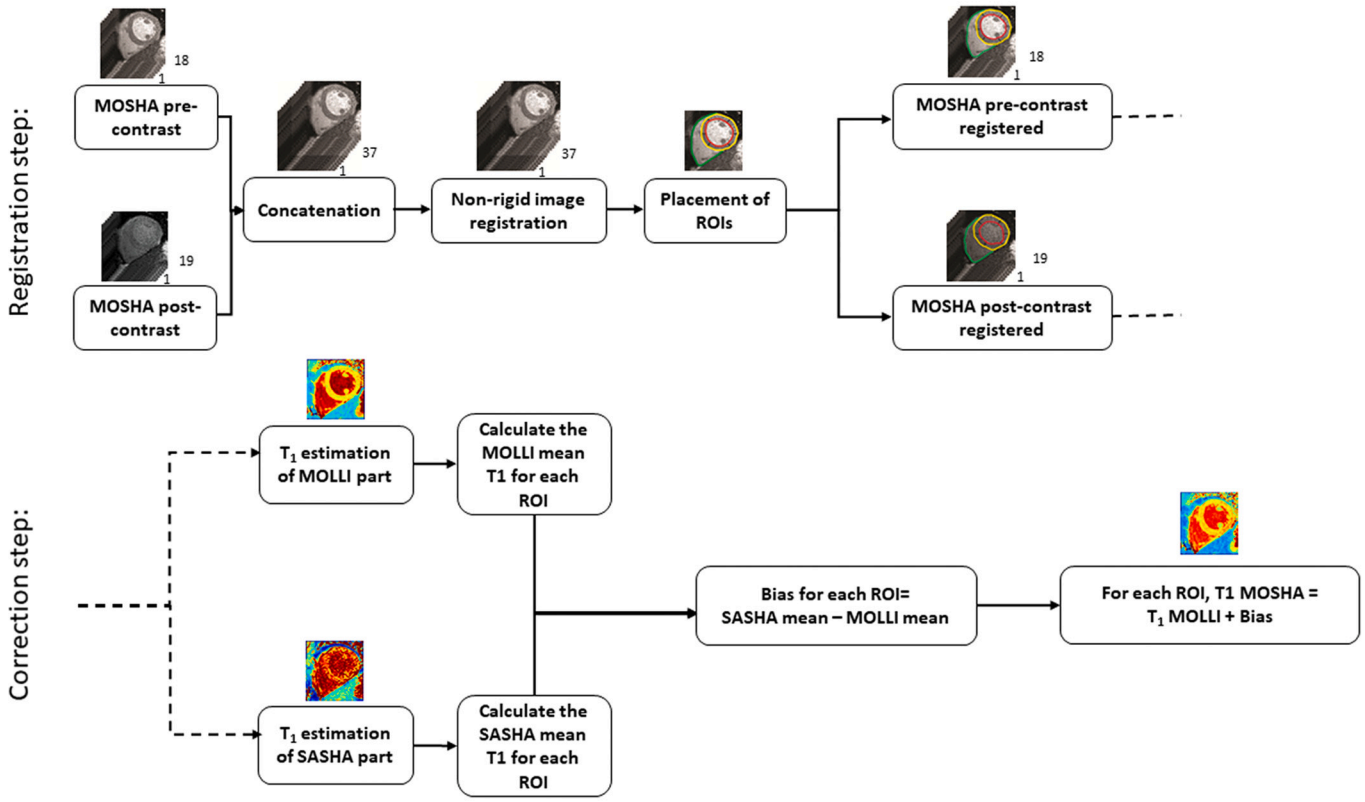

Fig. 2. Calculation of T_1 using MOSHA images in the human study. In the registration step, a non-rigid image registration is performed to compensate for a possible respiratory motion drift and to MOLLI and SASHA images. Three regions of interest (ROI) are placed in the LV blood pool, RV blood pool, and the LV myocardium. In the correction step for each patient, images are divided into the MOLLI and SASHA parts, and T_1 maps are then estimated for each. The average value over each ROI is calculated. The bias in T_1 estimation is calculated as the difference between the average T_1 value from SASHA and MOLLI images for each ROI for each patient individually. Finally, a MOSHA T_1 map is generated by adding the calculated bias to the T_1 map generated from MOLLI part.

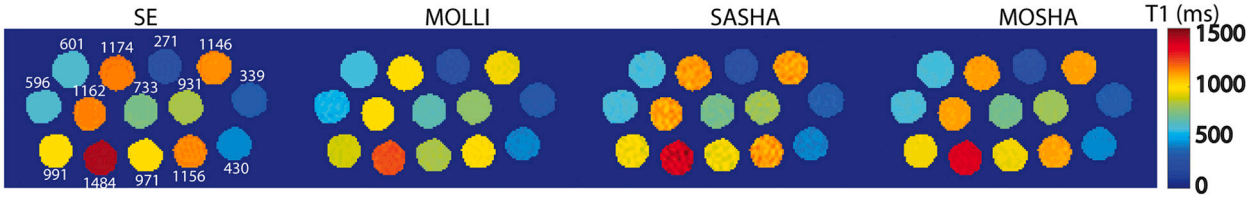

Fig. 3. Phantom study pre-contrast T_1 maps based on SE (reference), MOLLI, SASHA, and MOSHA images. The mean T1 value for each tube is shown by a color scale and listed for the SE image. More color homogeneity in each tube means better precision and T_1 values closer to SE means better accuracy. MOLLI had good precision but reduced accuracy. SASHA had better accuracy but lower precision. MOSHA had both good accuracy and precision.

coarctation of the aorta ($n = 5$), atrial septal defect ($n = 3$), aortic stenosis (n = 3), myocarditis ($n = 2$), myotonic dystrophy ($n = 1$), and superior sinus venosus defect (n = 1). All successfully completed the acquisition of pre- and post-contrast MOLLI, SASHA, and MOSHA images. The mean heart rate during the CMR scan was 72 ± 10 bpm. Figs. 5 and 6 show the pre- and post-contrast T_1 maps and synthetic ECV maps generated from MOLLI, SASHA, and MOSHA images acquired from 2 patients.

Two sets of pre- and post-contrast MOLLI, SASHA, and MOSHA images were acquired in each patient. The pre- and post-contrast mean T_1 in the LV blood pool, RV blood pool, and LV myocardium calculated from MOLLI, SASHA, and MOSHA images for the 15 patients are listed in Table 2. There was no significant difference (all P-values≥0.09) between MOSHA versus SASHA estimations of T_1 for the pre- and post-contrast values of LV blood pool, RV blood pool, and LV myocardium.

The mean standard deviation of T_1 pre- and post-contrast in the LV blood pool, RV blood pool, and LV myocardium calculated from MOLLI, SASHA, and MOSHA images for the 15 patients are listed in Table 3. For pre-contrast, the mean standard deviation of T_1 of MOSHA was significantly higher than that of MOLLI for the LV blood pool (170 ± 24 ms vs. 146 ± 26 ms; P-value<0.01) and for the RV blood pool (155 ± 33 ms vs. 136 ± 28 ms; P-value<0.01) but there was no difference for the LV myocardium (97 ± 30 ms vs. 92 ± 27 ms; P-value = 0.24). For post-contrast, the precision of MOSHA was significantly better than that of MOLLI for the LV blood pool (34 ± 6 ms vs. 50 ± 21 ms; P-value = 0.01) and the RV blood pool (27 ± 8 ms vs. 37 ± 11 ms; P-value<0.01), but there was no significant difference for the LV myocardium (42 ± 10 ms vs. 49 ± 18 ms; P-value = 0.07).

The mean LV synthetic ECV and standard deviation for LV synthetic ECV measured from MOLLI, SASHA, and MOSHA images are shown in Table 4. The mean synthetic ECV calculated by MOSHA was significantly lower than by MOLLI (26.0 ± 5.1% vs. 30.4 ± 6.1%; P-value<0.01) and comparable to SASHA (26.0 ± 5.1% vs. 25.7 ± 9.5%; P-value = 0.56). The standard deviation of synthetic ECV by MOSHA was significantly better than MOLLI (5.1 ± 1.5% vs. 6.1 ± 1.4%; P-value = 0.01) and SASHA (5.1 ± 1.5% vs. 9.5 ± 1.5%; P-value<0.01).

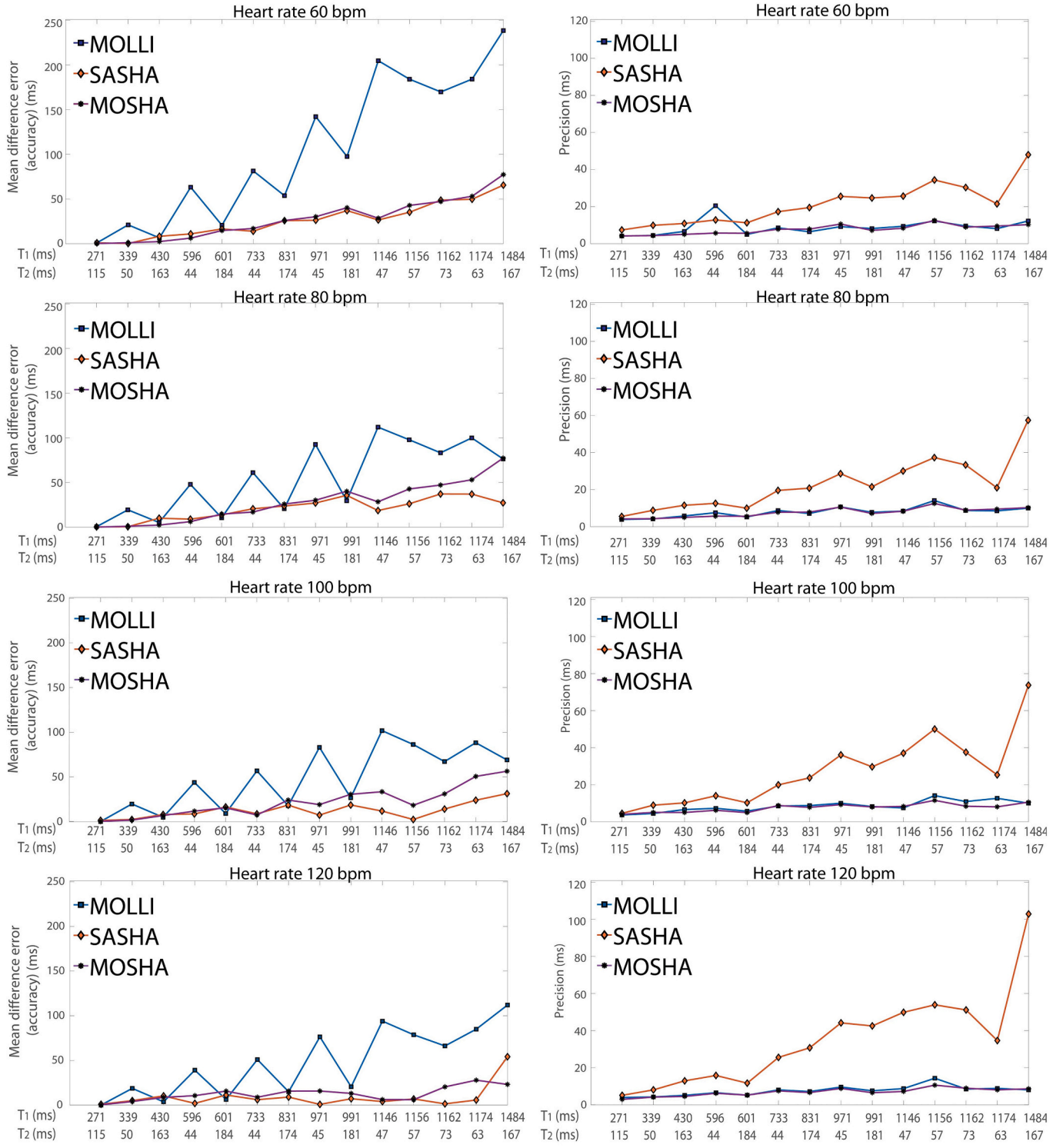

Fig. 4. Comparison of accuracy and precision for pre-contrast between MOLLI, SASHA, and MOSHA images for heart rates of 60, 80, 100, and 120 bpm.

Table 1
The mean difference error (a measure of accuracy) and the standard deviation (a measure of precision) for T_1 measurement using data from all heart rates and SE T_1 values as a reference.

	MOLLI	SASHA	MOSHA
Mean difference error (ms)	63.7 ± 55.5	13.2 ± 18.5	14.1 ± 42.1
Standard deviation (ms)	8.2 ± 3.1	26.6 ± 18.5	8.6 ± 4.9

Values are mean ± standard deviation.

Supporting Fig. 3 shows the Bland-Altman plots comparing the pre-contrast T_1 values calculated from SASHA and MOSHA, and MOLLI and MOSHA images at myocardium and blood pools in the LV and RV cavities. Supporting Fig. 4 display the Bland-Altman plots comparing the post-contrast T_1 values calculated from SASHA and MOSHA, and MOLLI and MOSHA images at myocardium and blood pools in the LV and RV cavities.

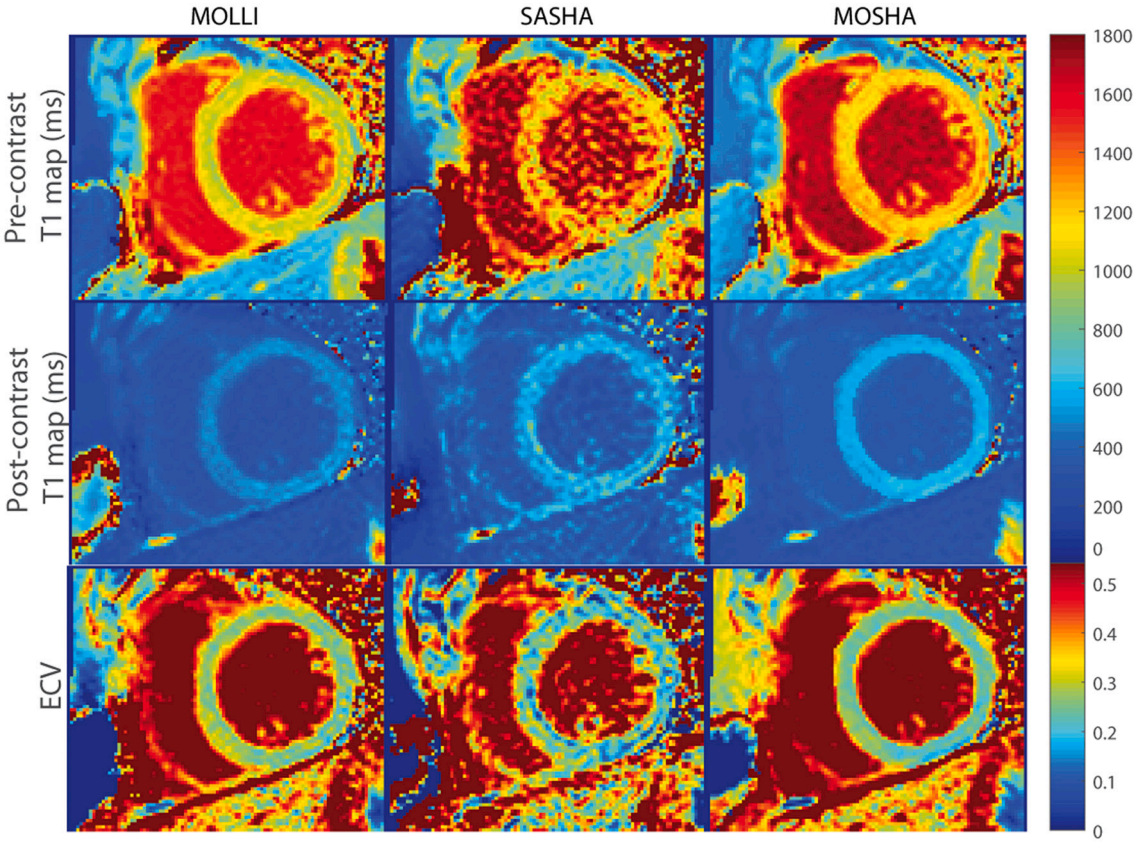

Fig. 5. T_1 and synthetic ECV maps in a 15-year-old female patient with a superior sinus venosus defect.

4. Discussion

We developed a new CMR T_1 mapping method, MOSHA, based on a combination of the MOLLI and SASHA sequences with the aim of achieving both accurate and precise measurements. It combines the previously recognized accuracy of the SASHA sequence with the precision of the MOLLI sequence. Calculation of the MOSHA T_1 in essence corrects the T_1 value derived from the MOLLI part of the sequence based on the T_1 value derived from the SASHA part of the sequence. If the MOLLI and SASHA sequences were acquired as two separate acquisitions, the results might be inferior to MOSHA. This is because patients may hold their breath differently for two acquisitions.

In the phantom study, MOLLI, SASHA, and MOSHA were compared to SE as the golden standard. MOSHA was shown to be as accurate as SASHA and as precise as MOLLI. In our patient study, SASHA was considered as the reference sequence for accuracy and MOLLI for precision. There was no significant difference between MOSHA and SASHA estimations of T_1 for pre- and post-contrast values of LV blood pool, RV blood pool, and LV myocardium. For both pre- and post-contrast acquisitions, the bias between the T_1 values calculated from SASHA and MOSHA images was $<2.6\%$ at myocardium, $<0.8\%$ at LV blood pool, and $<1.8\%$ for RV blood pool. The precision of MOSHA estimations of T_1 was similar to or better than that of MOLLI for pre- and post-contrast values of LV blood pool, RV blood pool, and LV myocardium. In the patient study, the difference between the precision of MOLLI part of MOSHA and MOLLI images in pre- and post-contrast could stem from different acquisitions resulting in different level of breath-holdings, heartrates, and ROIs for the ventricles and myocardium. For synthetic ECV the precision of MOSHA was significantly better than MOLLI and similar to SASHA.

Although the MOLLI sequence is less accurate than the SASHA sequence for T_1 and ECV measurement, it is widely used in clinical practice because it is more precise than SASHA [10]. It has been shown that MOLLI underestimates T_1 [15,16,23], is dependent on T_2, and is sensitive to magnetization transfer [16,19]. This inaccuracy of MOLLI affects the ECV measurement as well. ECV measurement cannot be accurate, because the T_1 maps being used are not accurate. In contrast, SASHA accurately estimates T_1, is T_2 independent, and is insensitive to magnetization transfer [24,25]. There have been many attempts to either improve the accuracy of MOLLI [1,6,8,13,26–29] or increase the precision of SASHA [1,5,30]. Saturation pulse prepared heart rate independent inversion recovery (SAPPHIRE) [31] yields similar accuracy as SASHA but its precision is lower than MOLLI [16]. It has been shown that ECV measurement with MOLLI is significantly different compared with SASHA and SAPPHIRE [16]. The ANGIE sequence [6] altered the MOLLI acquisition scheme by skipping one or more heartbeats to allow more recovery time between pre-pules but it still did not reach the precision of MOLLI. Hybrid methods using inversion and saturation recovery pre-pulses at the same time [12,14] have also been tried to minimize the MOLLI sequence's shortcomings. Although these techniques achieve the accuracy of SASHA, they are still not as precise as MOLLI [16]. Furthermore, there are a number of free-breathing methods based on either saturation [30,32] or inversion recovery [10,28,33,34] pre-pulses that try to improve the precision of SASHA or the accuracy of MOLLI. Some of these free-breathing methods could achieve a similar accuracy to breath-hold SASHA while maintaining the same precision as MOLLI [30,32].

Our study has several limitations. The patient population was small and it is thus possible that additional differences among the MOSHA, SASHA, and MOLLI sequences might emerge with larger sample size. Recruitment of healthy subjects for a contrast-enhanced CMR exam was not possible in our institution. In addition, breath-holding was used for respiratory motion compensation. Patients who are too young or ill may not be able to hold their breath for ≈21 s assuming a heart rate of 60

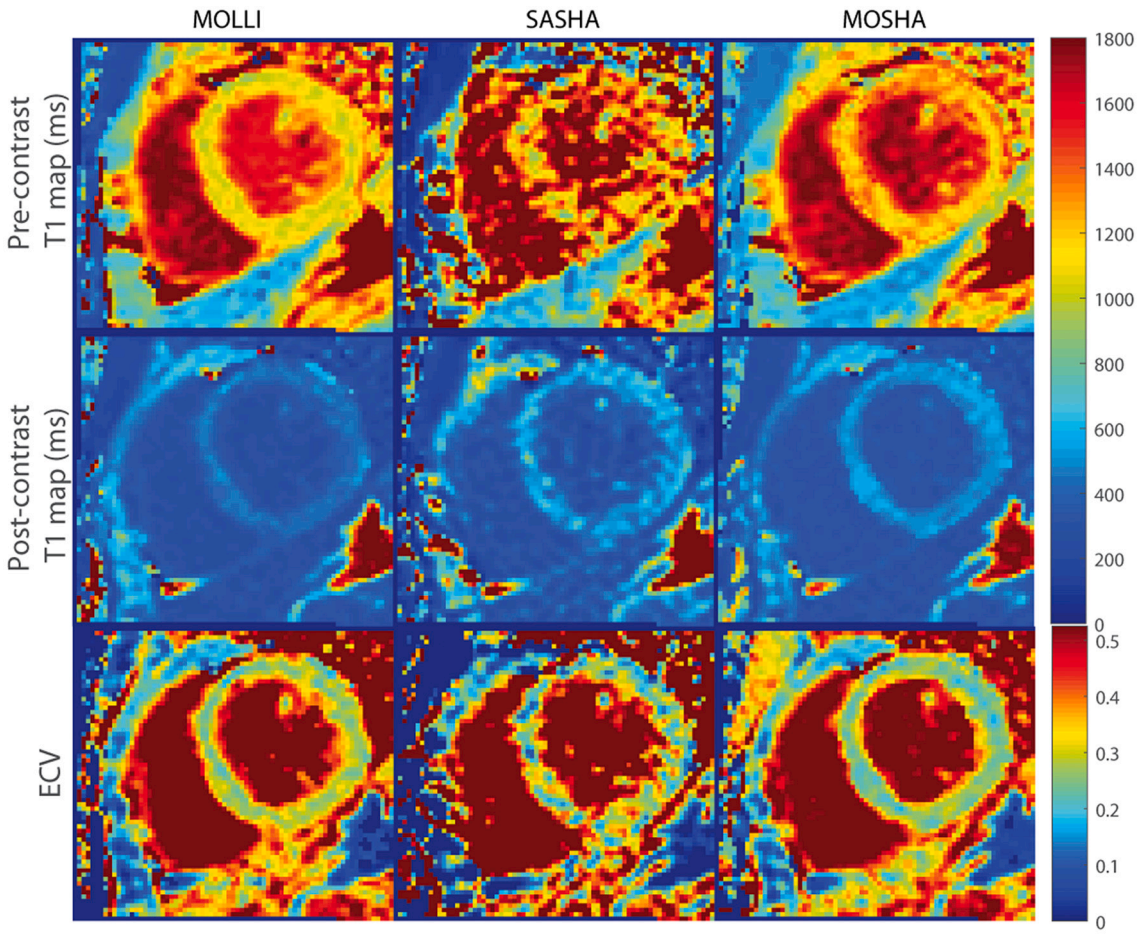

Fig. 6. T_1 and synthetic ECV maps in a 20-year-old female patient with bicuspid aortic valve.

Table 2
Estimated pre- and post-contrast T_1 values using MOLLI, SASHA, and MOSHA images in 15 patients.

	Pre-contrast					Post-contrast				
	MOLLI	SASHA	MOSHA	SASHA vs. MOSHA *P*-value	MOLLI vs. MOSHA *P*-value	MOLLI	SASHA	MOSHA	SASHA vs. MOSHA *P*-value	MOLLI vs. MOSHA *P*-value
LV blood pool (ms)	1414 ± 450	1489 ± 60	1501 ± 53	0.21	<0.01	354 ± 41	391 ± 45	391 ± 42	0.98	<0.01
RV blood pool (ms)	1431 ± 109	1493 ± 88	1520 ± 71	0.10	<0.01	351 ± 53	393 ± 64	391 ± 60	0.70	<0.01
LV myocardium (ms)	1047 ± 24	1257 ± 45	1230 ± 51	0.70	<0.01	451 ± 38	584 ± 49	569 ± 40	0.09	<0.01

Values are mean ± standard deviation.

Table 3
Standard deviation of the estimated pre- and post-contrast T_1 values using MOLLI, SASHA, and MOSHA images in 15 patients.

	Pre-contrast					Post-contrast				
	MOLLI	SASHA	MOSHA	SASHA vs. MOSHA *P*-value	MOLLI vs. MOSHA *P*-value	MOLLI	SASHA	MOSHA	SASHA vs. MOSHA *P*-value	MOLLI vs. MOSHA *P*-value
LV blood pool (ms)	146 ± 26	228 ± 25	170 ± 24	<0.01	<0.01	50 ± 21	95 ± 26	34 ± 6	<0.01	0.01
RV blood pool (ms)	136 ± 28	240 ± 52	155 ± 33	<0.01	<0.01	37 ± 11	78 ± 22	27 ± 8	<0.01	<0.01
LV myocardium (ms)	92 ± 27	232 ± 28	97 ± 30	<0.01	0.24	49 ± 18	105 ± 20	42 ± 10	<0.01	0.07

Values are mean ± standard deviation.

Table 4
Mean LV synthetic ECV percentage and standard deviation of synthetic ECV percentage calculated from MOLLI, SASHA, and MOSHA images in 15 patients.

	MOLLI	SASHA	MOSHA	SASHA vs. MOSHA *P*-value	MOLLI vs. MOSHA *P*-value
Mean of synthetic ECV%	30.4 ± 6.1	25.7 ± 9.5	26.0 ± 5.1	0.56	<0.01
Standard deviation of synthetic ECV%	6.1 ± 1.4	9.5 ± 1.5	5.1 ± 1.5	<0.01	0.01

Values are mean ± standard deviation.

bpm resulting in respiratory motion artifacts including through-plane motion that cannot be adequately compensated for with an image registration algorithm. To address this, MOSHA could also be acquired with free-breathing techniques [10,30,32–34]. Dictionary matching algorithms [35], instead of exponential fitting, or image denoising [36] could also be used to reduce the number of heartbeats, and acquisition time. In addition, we did not compare the performance of MOSHA that needs a long breath-hold of 21 s with the combination of MOLLI and SASHA sequences that are acquired in two different scans with a shorter breath-hold time. Furthermore, we did not study the impact of flip angle on improving the precision of SASHA and SASHA part of MOSHA. We used the flip angle of 35° for the SASHA acquisitions [10]; however, a higher flip angle could be used to increase the accuracy of SASHA [16]. Finally, we did not explore the effect of the first image acquisition without a pre-pulse in the MOSHA sequence on MOLLI part of the MOSHA. This acquisition could potentially affect the T_1 measurements in MOLLI part of the MOSHA; however, this effect is compensated for by using the SASHA part of the MOSHA as shown in the phantom study.

5. Conclusion

We developed a new T_1 mapping sequence, MOSHA, for an accurate and precise estimation of T_1 and synthetic ECV maps for CMR exams. Accuracy of MOSHA was similar to SASHA and its precision was as good as MOLLI. Such a sequence could be an alternative to MOLLI since it provides both accurate and precise T_1 maps and ECV values. Future efforts will focus on making the MOSHA technique free-breathing and faster by modifying MOLLI and SASHA schemes.

Supplementary data to this article can be found online at https://doi.org/10.1016/j.mri.2022.02.004.

CRediT authorship contribution statement

Majid Sohani: Conceptualization, Data curation, Formal analysis, Investigation, Methodology, Software, Validation, Visualization, Writing – original draft, Writing – review & editing. **Rob J. van der Geest:** Data curation, Formal analysis, Visualization, Writing – review & editing. **Andreas Maier:** Conceptualization, Writing – review & editing. **Andrew J. Powell:** Visualization, Writing – original draft, Writing – review & editing. **Mehdi H. Moghari:** Conceptualization, Data curation, Formal analysis, Investigation, Methodology, Software, Validation, Funding acquisition, Project administration, Resources, Supervision, Visualization, Writing – original draft, Writing – review & editing.

Acknowledgment

The authors would like to thank the patients for their participation in our study and our technologists (Stephanie Agudelo, Kinsey Brassaw, James Connors, Maria Valenza, and David Annese) for recruiting and scanning the patients. This work was supported by the German Academic Exchange Service or DAAD (Deutscher Akademischer Austauschdienst).

References

[1] Kellman P, Hansen MS. T1-mapping in the heart: accuracy and precision. J Cardiovasc Magn Reson 2014;16:2.
[2] Haaf P, Garg P, Messroghli DR, Broadbent DA, Greenwood JP, Plein S. Cardiac T1 mapping and extracellular volume (ECV) in clinical practice: a comprehensive review. J Cardiovasc Magn Reson 2016;18(1):89.
[3] Radenkovic D, Weingartner S, Ricketts L, Moon JC, Captur G. T1 mapping in cardiac MRI. Heart Fail Rev 2017;22(4):415–30.
[4] Kim PK, Hong YJ, Im DJ, Suh YJ, Park CH, Kim JY, et al. Myocardial T1 and T2 mapping: techniques and clinical applications. Korean J Radiol 2017;18(1):113–31.
[5] Akcakaya M, Weingartner S, Basha TA, Roujol S, Bellm S, Nezafat R. Joint myocardial T1 and T2 mapping using a combination of saturation recovery and T2-preparation. Magn Reson Med 2016;76(3):888–96.
[6] Mehta BB, Chen X, Bilchick KC, Salerno M, Epstein FH. Accelerated and navigator-gated look-locker imaging for cardiac T1 estimation (ANGIE): development and application to T1 mapping of the right ventricle. Magn Reson Med 2015;73(1):150–60.
[7] Messroghli DR, Radjenovic A, Kozerke S, Higgins DM, Sivananthan MU, Ridgway JP. Modified look-locker inversion recovery (MOLLI) for high-resolution T1 mapping of the heart. Magn Reson Med 2004;52(1):141–6.
[8] Piechnik SK, Ferreira VM, Dall'Armellina E, Cochlin LE, Greiser A, Neubauer S, et al. Shortened Modified Look-Locker Inversion recovery (ShMOLLI) for clinical myocardial T1-mapping at 1.5 and 3 T within a 9 heartbeat breathhold. J Cardiovasc Magn Reson 2010;12:69.
[9] Santini F, Kawel-Boehm N, Greiser A, Bremerich J, Bieri O. Simultaneous T1 and T2 quantification of the myocardium using cardiac balanced-SSFP inversion recovery with interleaved sampling acquisition (CABIRIA). Magn Reson Med 2015;74(2):365–71.
[10] Weingartner S, Roujol S, Akcakaya M, Basha TA, Nezafat R. Free-breathing multislice native myocardial T1 mapping using the slice-interleaved T1 (STONE) sequence. Magn Reson Med 2015;74(1):115–24.
[11] Chow K, Flewitt JA, Green JD, Pagano JJ, Friedrich MG, Thompson RB. Saturation recovery single-shot acquisition (SASHA) for myocardial T(1) mapping. Magn Reson Med 2014;71(6):2082–95.
[12] Song T, Stainsby JA, Ho VB, Hood MN, Slavin GS. Flexible cardiac T1 mapping using a modified look-locker acquisition with saturation recovery. Magn Reson Med 2012;67(3):622–7.
[13] Huang L, Neji R, Nazir MS, Whitaker J, Reid F, Bosio F, et al. Fast myocardial T1 mapping using shortened inversion recovery based schemes. J Magn Reson Imaging 2019;50(2):641–54.
[14] Weingartner S, Akcakaya M, Basha T, Kissinger KV, Goddu B, Berg S, et al. Combined saturation/inversion recovery sequences for improved evaluation of scar and diffuse fibrosis in patients with arrhythmia or heart rate variability. Magn Reson Med 2014;71(3):1024–34.
[15] Weingartner S, Messner NM, Budjan J, Lossnitzer D, Mattler U, Papavassiliu T, et al. Myocardial T1-mapping at 3T using saturation-recovery: reference values, precision and comparison with MOLLI. J Cardiovasc Magn Reson 2016;18(1):84.
[16] Roujol S, Weingartner S, Foppa M, Chow K, Kawaji K, Ngo LH, et al. Accuracy, precision, and reproducibility of four T1 mapping sequences: a head-to-head comparison of MOLLI, ShMOLLI, SASHA, and SAPPHIRE. Radiology 2014;272(3):683–9.
[17] Klein S, Staring M, Murphy K, Viergever MA, Pluim JP. Elastix: a toolbox for intensity-based medical image registration. IEEE Trans Med Imaging 2010;29(1):196–205.
[18] Tao Q, van der Tol P, Berendsen FF, Paiman EHM, Lamb HJ, van der Geest RJ. Robust motion correction for myocardial T1 and extracellular volume mapping by principle component analysis-based groupwise image registration. J Magn Reson Imaging 2018;47(5):1397–405.
[19] Cameron D, Vassiliou VS, Higgins DM, Gatehouse PD. Towards accurate and precise T 1 and extracellular volume mapping in the myocardium: a guide to current pitfalls and their solutions. MAGMA 2018;31(1):143–63.
[20] Flett AS, Hayward MP, Ashworth MT, Hansen MS, Taylor AM, Elliott PM, et al. Equilibrium contrast cardiovascular magnetic resonance for the measurement of diffuse myocardial fibrosis: preliminary validation in humans. Circulation 2010;122(2):138–44.
[21] Treibel TA, Fontana M, Maestrini V, Castelletti S, Rosmini S, Simpson J, et al. Automatic measurement of the myocardial Interstitium: synthetic extracellular volume quantification without hematocrit sampling. JACC Cardiovasc Imaging 2016;9(1):54–63.
[22] Kellman P, Arai AE, Xue H. T1 and extracellular volume mapping in the heart: estimation of error maps and the influence of noise on precision. J Cardiovasc Magn Reson 2013;15(1):56.
[23] Hamilton-Craig CR, Strudwick MW, Galloway GJ. Cardiac Magnetic Resonance T1 Mapping in Cardiomyopathies. 2017.
[24] Chow K, Flewitt J, Pagano JJ, Green JD, Friedrich MG, Thompson RB. T2-dependent errors in MOLLI T1 values: simulations, phantoms, and in-vivo studies. J Cardiovasc Magn Reson 2012;14(1):P281.
[25] Robson MD, Piechnik SK, Tunnicliffe EM, Neubauer S. T1 measurements in the human myocardium: the effects of magnetization transfer on the SASHA and MOLLI sequences. Magn Reson Med 2013;70(3):664–70.
[26] Messroghli DR, Greiser A, Frohlich M, Dietz R, Schulz-Menger J. Optimization and validation of a fully-integrated pulse sequence for modified look-locker inversion-recovery (MOLLI) T1 mapping of the heart. J Magn Reson Imaging 2007;26(4):1081–6.

[27] Wetzl J, Stalder AF, Schmidt M, Akgök YH, Tillmanns C, Lugauer F, et al. Joint Estimation of Cardiac Motion and T1 Maps for Magnetic Resonance Late Gadolinium Enhancement Imaging. 2016.
[28] Wang X, Joseph AA, Kalentev O, Merboldt KD, Voit D, Roeloffs VB, et al. High-resolution myocardial T1 mapping using single-shot inversion recovery fast low-angle shot MRI with radial undersampling and iterative reconstruction. Br J Radiol 2016;89(1068):20160255.
[29] Kvernby S, Warntjes M, Engvall J, Carlhall CJ, Ebbers T. Clinical feasibility of 3D-QALAS - single breath-hold 3D myocardial T1- and T2-mapping. Magn Reson Imaging 2017;38:13–20.
[30] Nordio G, Bustin A, Henningsson M, Rashid I, Chiribiri A, Ismail T, et al. 3D SASHA myocardial T1 mapping with high accuracy and improved precision. MAGMA 2019;32(2):281–9.
[31] Weingärtner S, Akcakaya M, Berg S, Kissinger KV, Manning WJ, Nezafat R. Heart-rate independent myocardial T1-mapping using combined saturation and inversion preparation pulses. J Cardiovasc Magn Reson 2013;15(Suppl. 1):P46.
[32] Chow K, Yang Y, Shaw P, Kramer CM, Salerno M. Robust free-breathing SASHA T1 mapping with high-contrast image registration. J Cardiovasc Magn Reson 2016;18(1):47.
[33] Weingartner S, Akcakaya M, Roujol S, Basha T, Stehning C, Kissinger KV, et al. Free-breathing post-contrast three-dimensional T1 mapping: volumetric assessment of myocardial T1 values. Magn Reson Med 2015;73(1):214–22.
[34] Tsai JM, Huang TY, Tseng YS, Lin YR. Free-breathing MOLLI: application to myocardial T(1) mapping. Med Phys 2012;39(12):7291–302.
[35] Henningsson M. Cartesian dictionary-based native T1 and T2 mapping of the myocardium. Magnetic Resonance in Medicine 2022;87(5):2347–62.
[36] Bustin A, Ferry P, Codreanu A, Beaumont M, Liu S, Burschka D, et al. Impact of denoising on precision and accuracy of saturation-recovery-based myocardial T1 mapping. J Magn Reson Imaging 2017;46(5):1377–88.